Computational Materials Science 44 (2008) 807–812

Contents lists available at ScienceDirect

Computational Materials Science

journal homepage: www.elsevier.com/locate/commatsci

New analytical model for local heat flux density in the mold in continuous casting of steel

Mostafa Alizadeh, Ahmad Jenabali Jahromi *, Omid Abouali

Department of Materials Science and Engineering, Shiraz University, Shiraz, Iran

ARTICLE INFO

Article history:
Received 13 August 2007
Received in revised form 23 May 2008
Accepted 27 May 2008
Available online 14 July 2008

PACS:
44.10.+i
44.05.+e
61.66.Dk
64.70.D–
81.30.Fb
81.05.–t

Keywords:
Continuous casting
Local heat flux
Numerical simulation
Meniscus
Manageable parameters

ABSTRACT

In this article, a model representing local heat flux density in the mold in continuous casting of steel is presented. This model is a modification for empirical model of Schwerdtfeger. A new parameter is defined as $LHTC_z$ (longitudinal heat transfer coefficient). The multiplication of $LHTC_z$ to total increase of the cooling water temperature (ΔT_w^T) leads to a new model for local heat flux density. Since ΔT_w^T is a measurable parameter, the present model can be used in on-line controlling of continuous casting process. Results of the present model were compared with the experimental data and a good agreement was seen. Also it was shown that present model can be used as a boundary condition in solidification numerical modeling.

1. Introduction

The continuous casting process has been mathematically modeled for more understanding of the important variables in the process, improve the design of continuous casting system, and eliminate casting defect [1]. The extant information in many investigations shows that the mold is a critical component of continuous casting machine [2–11]. Heat transfer in the mold plays a critical role on productivity and quality of steel [12]. The efficiency of heat extraction in the mold is ultimately responsible for the surface quality of the cast product and the productivity of the machine [13]. So some investigators have used the local heat flux density as a defect indicator [14,15]. Moreover in solidification modeling, to predict the temperature and thickness of the solidified shell, local heat flux density is needed as a boundary condition in numerical solution of the heat conduction equation [16].

The heat transfer character in the mold region has a complex behavior. The heat transfer at the mold is controlled by [17]:

- Convection of superheat of the liquid to the shell surface.
- Solidification (latent heat evolution in the mushy zone).
- Conduction through the solid shell.
- The properties of the thermal resistance (mold flux and gas gap) which have filled the gap between the solidified shell and the mold [18–24].
- Conduction through the copper mold and convection to the cooling water.

The greatest difficulty in accurate heat flow modeling is determination of the heat transfer across the gap between the solidified shell and mold, because it is controlled by the thickness and properties of the mold flux and gas gap at a given time [17]. Such measurements of the heat flux density are performed by determination of the temperature gradients in the copper plate of the mold, and by measuring the temperature increase in the cooling water [25]. Usually molds instrumented with thermocouples are used for measurement of local heat flux density, and the total increase in the cooling water temperature is used for measurement of the average heat flux density [16,26–28]. The main parameter influencing the heat withdrawal in the mold is the casting velocity, but there are several other factors such as the taper of the mold, the type of

* Corresponding author. Tel./fax: +987112307293.
E-mail addresses: alizadehm@shirazu.ac.ir (M. Alizadeh), jahromi@shirazu.ac.ir (A. Jenabali Jahromi), abouali@shirazu.ac.ir (O. Abouali).

0927-0256/$ - see front matter © 2008 Elsevier B.V. All rights reserved.
doi:10.1016/j.commatsci.2008.05.034

Nomenclature

A	apparent heat flux density at the meniscus if V_C = 1 m min^{-1}
C_w	specific heat of water at average temperature of water in the mold length (J kg^{-1} K^{-1})
$C(T)$	temperature depended specific heat of steel (J kg^{-1} K^{-1})
ds	differential control surface on the mold surface (m^2)
dz	height of the differential control surface (m)
f_s	solid fraction
H_m	mold length (m)
H_{me}	mold length in contact to the melt (m)
$H(T)$	enthalpy of the material (J kg^{-1})
h	sensible enthalpy (J kg^{-1})
$k(T)$	temperature dependent conductivity of steel (W m^{-1} K^{-1})
LHTC$_z$	longitudinal heat transfer coefficient (W m^{-2} K^{-1})
P_m	perimeter of the tube mold (for billet and bloom) or the width of slab (m)
Q	volume flow rate of cooling water (m^3 s^{-1})
q	local heat flux density (W m^{-2})
q_a	apparent heat flux density at the meniscus (W m^{-2})
$\dot{q}$	latent heat source (W m^{-3})
$\bar{q}$	average heat flux density absorbed by cooling water (W m^{-2})
T_w^0	initial water temperature (°C)
T_w	water temperature at a given distance from meniscus
t	time (s)
t_T	transit time (s)
V_C	casting velocity (m s^{-1})
x, y	rectangular coordinates (m)
α	experimental exponent in Eq. (1) (m^{-1})
ΔH_f	heat of fusion (J kg^{-1})
ΔT_w^T	total increase of the cooling water temperature (°C)
ΔT_w	local increase of the cooling 3water temperature at the mold length (°C)
ρ_w	density of water at average temperature in the mold length (kg m^{-3})
$\rho(T)$	temperature depended density of steel (kg m^{-3})

the mold (e.g., straight and curved), the type of the lubricant, the composition of the steel (e.g., carbon content) and the superheat of the liquid. Some of these parameters are more important and others are less. There are several practical and useful correlations for local heat flux density obtained by measuring the temperature distribution in the mold wall. But only time parameter appeared in these correlations and this is the major limitation of these correlations [16].

The aim of this work is to present a correlation which includes important practical and controllable parameters such as mold level, cooling water volume flow rate and total increase in cooling water temperature. This work is based on Schwerdtfeger equation because it has been correlated with the plant data of billet, bloom and slab. Also this correlation includes the local heat flux density at the meniscus which is a function of some operational parameters such as casting velocity and machine characteristics.

2. Local heat flux density in the mold based on experimental data

Schwerdtfeger et al. [29] found, with a good approximation, that the local heat flux density behavior can be considered as straight lines in half-logarithmic plots of q against z. Hence, q can be described, for the normal operation, by the exponential law:

$$q = q_a e^{-\alpha z}. \quad (1)$$

The exponent α is obtained from the slope of the straight lines. The heat flux density at the meniscus (q_a) cannot be measured directly with the usual technique (determination of temperature gradient with two thermocouples) because the temperature field in the copper plate is strongly two-dimensional in this region, causing a considerable longitudinal heat flow upward to the cold top of the mold. However, q_a can be obtained by extrapolation to $z = 0$ from the straight lines in half-logarithmic plots of q as a function of z (in which q is obtained by experimental measuring). Schwerdtfeger et al. [12] determined q_a by this method at various casting velocity and plotted q_a as a function of V_C in log–log scale and presented following equation for q_a:

$$q_a = AV_C^{0.56}. \quad (2)$$

The quantity A depends on additional parameters and varies considerably for different machines and casting practices. Hence, for the mold heat flux density the equation is

$$q = AV_C^{0.56} e^{-\alpha z}. \quad (3)$$

In Eq. (3) only the casting velocity has appeared and the effects of other parameters such as mold dimensions, mold level, solidified shell thickness, mold flux, gas gap and the mold wall are hidden in A parameter. The measurement of the A, especially as on-line measuring, is very difficult because of the simultaneous effects of various parameters. The major limitation of this equation is the complexity of the measurement of q_a. In this work a correlation for the local heat flux density is presented which includes manageable parameters on a live mold such as total increase in cooling water temperature which is affected by mold flux, gas gap, steel composition and the mold wall.

3. Modification of the local heat flux density

Eq. (3) is a reliable rule, because it has been based on lots of experimental data of the slabs, blooms and billets [30]. An on-line controllable heat flux should be explained by the mold temperature profile or the cooling water temperature profile. Practically identification of the total increase in the cooling water temperature (ΔT_w^T) is easier than identification of mold temperature profile. However the ΔT_w^T is a global temperature increase at the mold length and it should be associated to local increase in the cooling water temperature at a given distance z from the meniscus. Similar to A in Eq. (2), ΔT_w^T is also affected by thermal heat resistances which practically detection of their effects on the heat flux is difficult. However, it seems using ΔT_w^T as a substitution for A in the heat flux relation simplifies the identification of A parameter.

Fig. 1 shows schematically the mold geometry and the thermal resistances against heat withdrawal from the mold. According to Fig. 1 the cooling water enters to the water jacket from the bottom of the mold at the volume rate of Q and temperature of T_w^0. The cooling water absorbs the heat flux from the mold and exits from top of the mold at $T_w^0 + \Delta t_w^T$.

The average heat flux density absorbed by cooling water ($\bar{q}$) can be computed using the total increase in cooling water temperature (ΔT_w^T) using following equation,

$$\bar{q} = \frac{\rho_w C_w Q \Delta T_w^T}{H_m P_m}. \quad (4)$$

For evaluation of the local heat flux density at a given distance from the meniscus, a differential control surface is considered on the mold surface, which can be displayed by

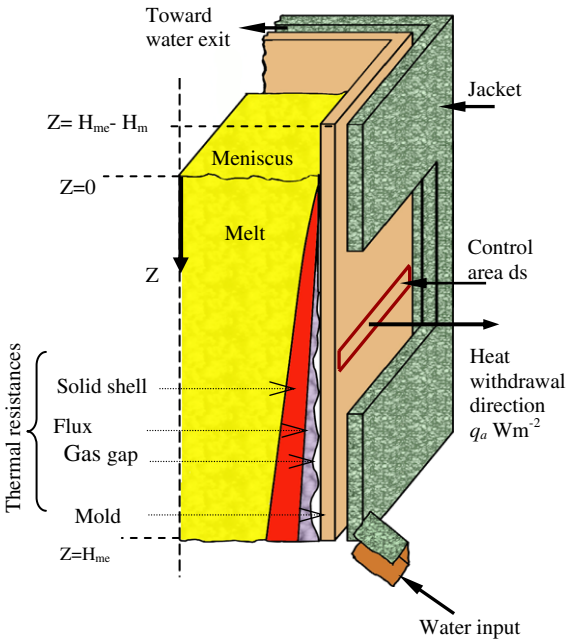

Fig. 1. Schematic of the mold geometry and thermal resistances against heat withdrawal from mold.

$$ds = dz \times P_m. \tag{5}$$

The local heat flux density in the differential control surface is as follows:

$$q = \frac{\rho_w C_w Q dT}{ds}. \tag{6}$$

The equality of Eqs. (1) and (6) leads to the temperature differential at the mold length via following relation:

$$\rho_w C_w Q dT = q_a e^{-\alpha z} ds \rightarrow dT = \frac{q_a P_m}{\rho_w C_w Q} \times e^{-\alpha z} dz. \tag{7}$$

The boundary conditions of Eq. (7) are:

$$\text{at} \quad z = H_{me} \quad \therefore \quad T_w = T_w^0 \rightarrow \Delta T_w = T_w^0 - T_w^0 = 0,$$

$$\text{at} \quad z = 0 \therefore \Delta T_w = \Delta T_w^T.$$

It is assumed that total temperature increase in water is equal to temperature difference of the water at the inlet of the mold and meniscus height. Because of increase in the cooling water temperature in the minus direction of intercept (see Fig. 1) a minus sign is added to Eq. (7) during integration.

$$\int_{T_w^0}^{T_w} dT = -\frac{q_a P_m}{\rho_w C_w Q} \int_{z=H_{me}}^{z} e^{-\alpha z} dz \rightarrow T_w - T_0^w = \Delta T_w$$
$$= \frac{P_m}{\alpha \rho_w C_w Q} (e^{-\alpha z} - e^{-\alpha H_{me}}) q_a. \tag{8}$$

By applying the second boundary condition, Eq. (8) leads to local heat flux density, as follows:

$$q_a = \frac{\alpha \rho_w C_w Q \Delta T_w^T}{P_m} \times \frac{1}{1 - e^{-\alpha H_{me}}}. \tag{9}$$

Substituting Eq. (9) in Eq. (8), we obtain the equation of local increase in cooling water temperature at the mold length as follows:

$$\Delta T_w = \Delta T_w^T \times \frac{e^{-\alpha z} - e^{-\alpha H_{me}}}{1 - e^{-\alpha H_{me}}} \tag{10}$$

Substituting Eq. (9) in Eq. (1), the equation of local heat flux density can be obtained via Eq. (11),

$$q(z) = \frac{\alpha \rho_w C_w Q \Delta T_w^T}{P_m} \times \frac{e^{-\alpha z}}{1 - e^{-\alpha H_{me}}}. \tag{11}$$

For easy notation of Eq. (11), a new parameter is defined as $LHTC_z$ (longitudinal heat transfer coefficient). $LHTC_z$ is the heat transfer coefficient of cooling water for increasing of water temperature from T_w^0 to T_w at a given distance from the meniscus. The subscript z shows that the value of $LHTC_z$ is different at the length of mold. $LHTC_z$ is shown as following,

$$LHTC_z = \frac{\alpha \rho_w C_w Q}{P_m} \times \frac{e^{-\alpha z}}{1 - e^{-\alpha H_{me}}}. \tag{12}$$

Therefore, the present model for the local heat flux density can be shown by Eq. (13)

$$q = \Delta T_w^T \times LHTC_z. \tag{13}$$

3.1. Evaluation of exponent α

The exponent α is the slope of straight lines in a half-logarithmic plot of q as a function of z or is the coefficient of z in Eq. (1). In this work, local heat flux density equations of slabs and billets were used, to evaluate the exponent α. Eqs. (14) [31] and (15) [30] for billets and Eqs. (16) [32] and (17) [28] for slabs have been obtained by fitting of many plant measurements by Thomas et al. in separate works. These empirical equations were used in this study to determine α exponent for slabs and billets by a regression method. The regression results in Fig. 2 show that α varies between 1 and 1.5. It is less than 1.25 m^{-1} for slabs and over 1.25 m^{-1} for billets.

$$q = 4,755,600(t)^{-0.504}, \tag{14}$$

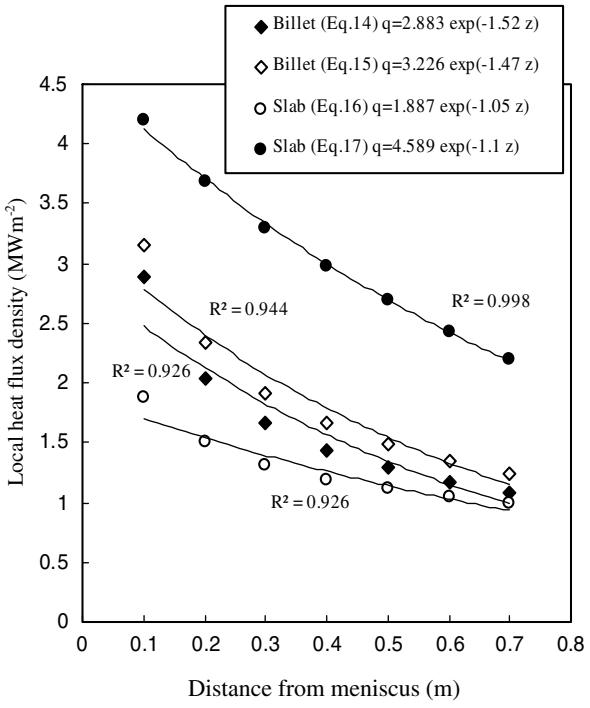

Fig. 2. Curve fitted equations (exponential form) of the local heat flux density for slabs and billets.

$$q = 6,500,000(t+1)^{-0.5}, \quad (15)$$

$$q = 2,710,000(t)^{-0.33}, \quad (16)$$

$$q = 5,403,000 - 990000(t)^{0.5}. \quad (17)$$

In these equations t is calculated by following equation:

$$t = 60z/V_C. \quad (18)$$

3.2. Evaluation of ΔT_w^T

The term of ΔT_w^T in the present heat flux model, Eq. (13), is measured directly by the continuous casting system. Naturally the measured ΔT_w^T has been affected by all of the effective parameters such as steel composition, condition of mold oscillation, casting velocity, mold level, mold taper, mold flux layer properties, gas gap properties and cooling water properties (water temperature and flow rate of cooling water). However in some applications for the local heat flux density (such as boundary condition in simulation of solidification) it is necessary to predict ΔT_w^T. A mathematical model for ΔT_w^T has been derived in another submitted paper by these authors.

4. Model validation

4.1. Comparison with experimental data

Konishi et al. [16] using the experimental data of Hiraki et al. [16] presented the following correlation for the heat flux at the meniscus:

$$q_a = 5,960,000\exp(-2.3t_T) + 1,490,000. \quad (19)$$

In Hiraki et al. [16] investigation, the heat flux was computed at a location 45 mm below the meniscus. Thus, in order to estimate the heat flux density at the meniscus, their data were modified by considering the transit time elapsed from the meniscus to the location of measurement. The transit time t_T, is given by the ratio of distance and casting speed, i.e.

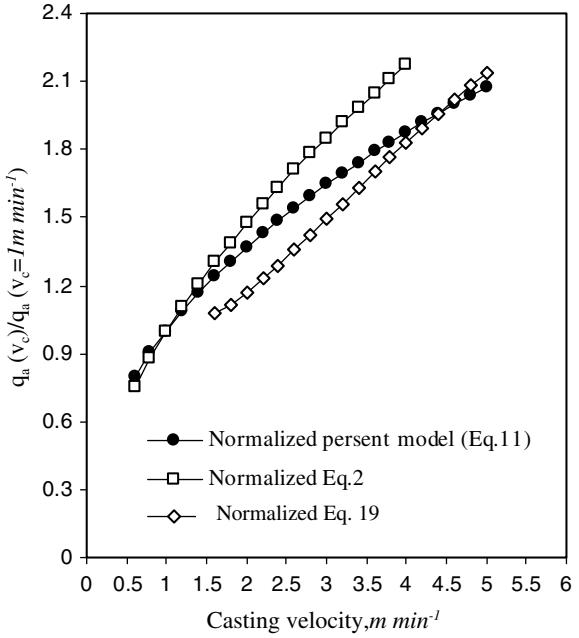

Fig. 3. Comparison between normalized forms of Eq. (2) (for casting velocity between 0.5 and 2.0 m min^{-1}), and Eq. (19) (for casting velocity about 5 m min^{-1}) and present model.

$$t_T = \frac{45}{V_C} \times \frac{60}{1000}. \quad (20)$$

Konishi et al. [16] fitted Eq. (19) for longitudinal crack modeling in slab. Fig. 3 compares the normalized form of present model (ratio of heat flux density at the meniscus at a given casting velocity to heat flux density at the meniscus for casting velocity equal one) with normalized form of Schwerdtfeger model (Eq. (2)) and normalized form of Konishi model (normalized form of Eq. (19)). The Schwerdtfeger model was presented based on experimental data for casting velocity less than 2 m min^{-1} and Konishi model for casting velocity about 5.0 m min^{-1}. Fig. 3 shows that the present model at low casting velocity with a good approximation corresponds to Schwerdtfeger model and at higher casting velocity corresponds to Konishi model. For this comparison the data of slab listed in Table 1 was used and α was considered equal to 1.25 m^{-1}.

Fig. 4 compares the local heat flux density for slab predicted by the present model (Eq. (11)) with the results of Eq. (1) in which Eq. (19) is used as q_a. For this comparison the data of slab which have been listed in Table 1 were used. In this comparison the exponent α was considered equal to 1.25 m^{-1}. Determination of Q from water velocity, selection of exponent α and curve fitting approximation could be the reasons for small difference between present model and empirical Eq. (19).

4.2. Validation of the model in simulation of solidification

In solidification modeling to predict the temperature and growth of the solidifying steel shell, the local heat flux is needed as a boundary condition in solution of heat conduction equation [16,27,33], therefore in this section the present model (Eq. (11)) is examined as a boundary condition for solidification modeling. For this purpose the numerical modeling of the strand has been developed to track a transverse slice of a steel bloom as it moves down through the mold. The mathematical formulation of heat transfer is based on the fundamental equation of heat conduction. Because of high heat extraction rate at the strand surface, heat conduction in z direction is negligible compared to the heat transferred by the bulk motion of strand [17]. Therefore, heat conduction equation reduces to a two-dimensional unsteady form [34]

$$\rho(T)C(T)\frac{\partial T}{\partial t} = \frac{\partial}{\partial x}\left(k(T)\frac{\partial T}{\partial x}\right) + \frac{\partial}{\partial y}\left(k(T)\frac{\partial T}{\partial y}\right) + \dot{q}, \quad (21)$$

$$\dot{q} = \rho(T)\Delta H_f \frac{\partial f_s}{\partial t}. \quad (22)$$

For simplification of Eqs. (21) and (22) the enthalpy formulation is used:

$$\frac{\partial \rho(T)H(T)}{\partial t} = \rho(T)C(T)\frac{\partial T}{\partial t} - \rho(T)\Delta H_f \frac{\partial f_s}{\partial t}. \quad (23)$$

The enthalpy of material is computed as the sum of sensible enthalpy, h, and the latent heat

$$H(T) = \left(h_{\text{ref}} + \int_{T\text{ref}}^{T} C(T)\mathrm{d}T\right) + f_s\Delta H_f. \quad (24)$$

The solid fraction is supposed to obey the linear model [35]:

$$f_s = \begin{cases} 1 & T < T_{\text{sol}} \\ \frac{T - T_{\text{liq}}}{T_{\text{sol}} - T_{\text{liq}}} & T_{\text{sol}} \leqslant T \leqslant T_{\text{liq}} \\ 0 & T_{\text{liq}} < T \end{cases}. \quad (25)$$

At the range of temperatures where solidification occurs for metallic alloys, the physical properties will be evaluated using following equations [36]:

Table 1
The practical conditions for numerical and analytical simulation of bloom and slab

Parameter	Bloom – 0.4% C (present work)	Slab – 0.04% C (Ref. [28])
Mold dimensions (m)	0.27 × 0.29	1.66 (width)
Mold length (m)	0.78	0.9
V_C (m min^{-1})	0.75	3.6
Mold level (%)	85	90 (working mold length 0.81 m)
Q (l min^{-1})	2347	4330
$T_{pouring}$ (°C)	1530	1550
T_{sol} (°C)	1396	1509
T_{liq} (°C)	1492	1529
k_l (W/mk)	39	39
k_s (W/mk)	(20.87 + 8.8345 × 10^{-3} T)	(20.87 + 8.8345 × 10^{-3} T)
C_l (J kg^{-1} K^{-1})	824.6157	824.6157
C_s (J kg^{-1} K^{-1})	(429.849 + 0.1498 × 10^{-3} T)	(429.849 + 0.1498×10^{-3} T)
ΔT_w^0 (°C)	4.9	10
ΔH_f (J kg^{-1})	260,000	272000
	T (°C)	T (°C)

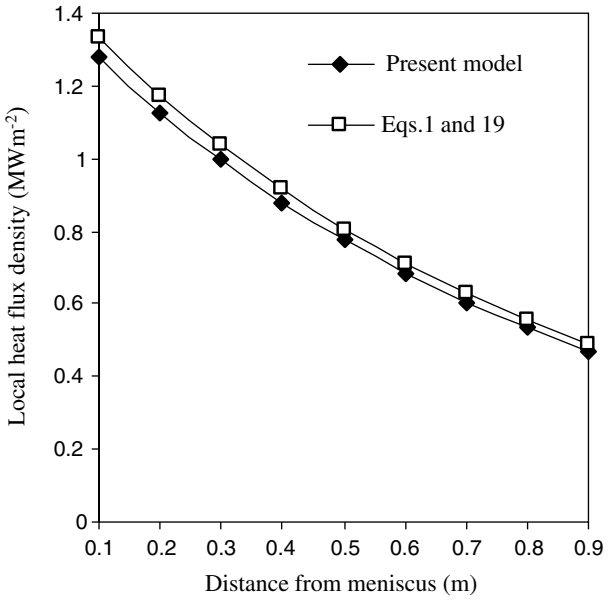

Fig. 4. Comparison of predicted local heat flux density by present model and combination of Konishi fitted equation with Eq. (1).

$$k = (k_S - k_L)f_s + k_L, \tag{26}$$

$$C = (C_S - C_L)f_s + C_L, \tag{27}$$

$$\rho = (\rho_S - \rho_L)f_s + \rho_L. \tag{28}$$

3.2.1. Boundary conditions

Fig. 5 shows the Schematic diagram of the coordinate and the computational domain. Two-dimensional heat transfer phenomenon was considered, with the heat flux being admitted to be negligible along the vertical direction (z), i.e., $\frac{\partial T}{\partial z} = 0$. The bloom symmetry permits that only one quarter of the cross-section is modeled for a full thermal evolution characterization. The boundary conditions are summary in below [36]:

$$\begin{aligned}
&\text{at} \quad y = 0 \quad \text{and} \quad 0 < x < x_s \quad -k(T)\tfrac{\partial T}{\partial y} = 0\\
&\text{at} \quad x = 0 \quad \text{and} \quad 0 < y < y_s \quad -k(T)\tfrac{\partial T}{\partial x} = 0\\
&\text{at} \quad y = y_s \quad \text{and} \quad 0 < x < x_s \quad -k(T)\tfrac{\partial T}{\partial y} = q\\
&\text{at} \quad x = x_s \quad \text{and} \quad 0 < y < y_s \quad -k(T)\tfrac{\partial T}{\partial x} = q\\
&\text{at} \quad t = 0 \quad T = T_{pouring}.
\end{aligned}$$

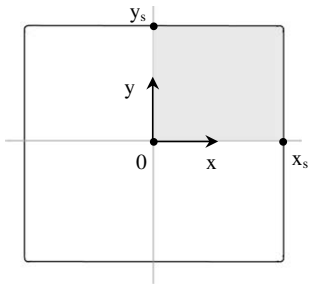

Fig. 5. The schematic diagram of coordinate and calculation domain.

The solid fraction used to measure solid shell thickness is equal to 0.75. The equations were solved using a finite volume code. The diffusive terms are discretized with a central-difference scheme and time derivative is discretized with a first-order implicit backward differences. The time step was set 0.05 s. The number of elements in generated uniform mesh was nearly 14,400. The case study which used in present numerical simulation is a bloom with breakout problem. Fig. 6 depicts the vertical breakout shell. The

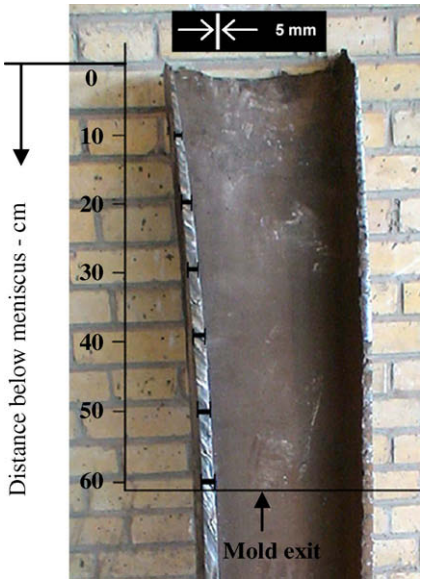

Fig. 6. The vertical breakout section which has happened in the fix sector area. This figure indicates the meniscus and the shell thickness along of the mold and below of the mold.

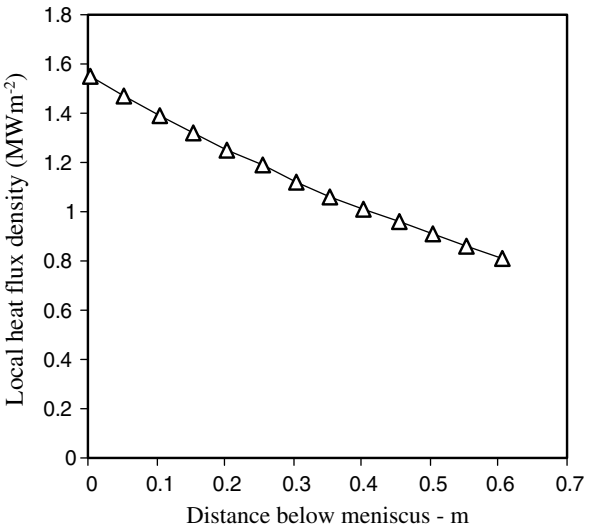

Fig. 7. The local heat flux density at the mold length for breakout bloom using listed data in Table 1.

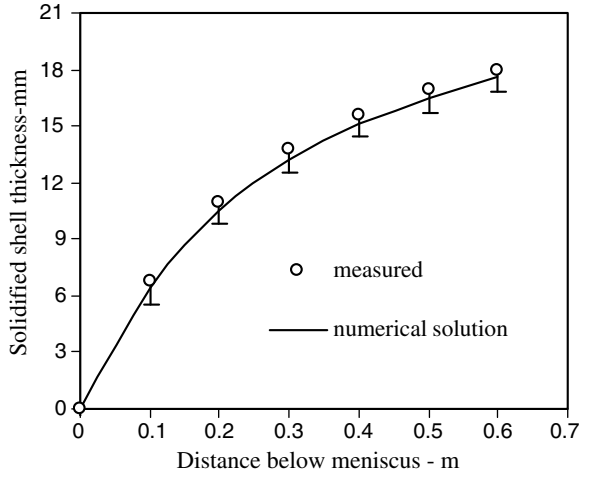

Fig. 8. Comparison of the measured and numerical predicted solidified shell. The present model (Eq. (11)) has been used as boundary condition in the numerical simulation.

measured thickness of solidified shell in the breakout shell was compared with the numerically computed shell thickness. Table 1 lists the practical conditions and mold characteristics for the bloom with breakout problem. Fig. 7 indicates the local heat flux density calculated by present model (Eq. (11)) at the mold length for breakout bloom. Fig. 8 compares the measured and numerical predicted solidified shell. As shown in Fig. 8, the present model as a boundary condition yields to a correct prediction of solidified shell. Fig. 8 shows that the simulated shell thickness using present model as a boundary condition is in reasonable agreement with the measured data. Therefore, the present model can be used as a boundary condition in the numerical solidification modeling. And it is possible to determine the effect of each operational parameter in the continuous casting process by numerical simulation of the solidification.

5. Conclusions

In this work a new model for local heat flux density in the continuous casting mold was presented. This model does not have the limitations of Schwerdtfeger model such as determination of q_a. The term of ΔT_w^T in present heat flux model, which is measured directly by the continuous casting system, has been affected by all effective parameters such as steel composition, condition of mold oscillation, casting velocity, mold level, mold taper, mold flux layer properties, gas gap properties and cooling water properties (water temperature and flow rate of cooling water). The present model can be used as a boundary condition in numerical simulation of solidification with a good accuracy. An advantage of present model is its controllability with manageable parameters i.e. casting velocity, flow rate of cooling water, and mold level.

Acknowledgement

The research reported in the present paper is supported by Iran Alloy Steel Company. The authors are grateful from that company.

References

[1] H.N. Han, J.E. Lee, T.J. Yeo, Y.M. Won, K.H. Kim, K.H. Oh, J.K. Yoon, ISIJ Int. 39 (5) (1999) 445–454.
[2] N. Chakraborti, R. Kumar, D. Jain, Appl. Math. Model. 25 (2001) 287–297.
[3] D.T. Stone, B.G. Thomas, Can. Metall. Q. 38 (5) (1999) 363–375.
[4] I.L. Ferreira, J.E. Spinelli, J.C. Pires, A. Garcia, Mater. Sci. Eng. A 408 (2005) 317–325.
[5] F. Lau, W.B. Lee, S.M. Xiong, B.C. Liu, J. Mater. Process. Technol. 79 (1998) 25–29.
[6] T. Li, K. Sassa, S. Asai, ISIJ Int. 36 (4) (1996) 410–416.
[7] H.M. Sahin, K. Kocatepe, R. Kaykc, N. Akar. Energy Convers. Manage. 47 (2006) 19–34.
[8] C.H. Yu, M. Suzuki, H. Shibata, T. Emi, ISIJ Int. 36 (1996) 159–162.
[9] J.W. Cho, H. Shibata, J. Non-Cryst. Solids 281 (2001) 110–117.
[10] F.C. Calzolari, I. Craig, C. Pistorius, ISIJ Int. 44 (8) (2004) 1393–1402.
[11] Y. Miki, S. Takeuchi, ISIJ Int. 43 (10) (2003) 1548–1555.
[12] Y. Hebi, Y. Man, J. Mater. Process. Technol. 183 (2007) 49–56.
[13] Y. Xie, H. Yu, X. Ruan, B. Wang, Y. Ma, J. Mater. Process. Technol. 99 (2008) 49–55.
[14] B.G. Thomas, Modeling of Continuous casting, in: A.W. Cramb (Ed.), The Making Shaping and Treating of Steel-Casting Volume, 11th ed., AISE Steel Foundation, Pittsburgh, 2003, p. 7.
[15] B.G. Thomas, Modeling, control and optimization in ferrous and nonferrous industry, in: F. Kongoli, B.G. Thomas, K. Sawamiphakdi (Eds.), Materials Science and Technology Symposium, Chicago, TMS, Warrendale, PA, 2003, pp. 29–45.
[16] J. Konishi, M. Militzer, J.K. Brimacombe, I.V. Samarasekera, Metall. Mater. Trans. B 33 (2002) 413–423.
[17] T. Emi, H. Fredriksson, Mater. Sci. Eng. A 413–414 (2005) 2–9.
[18] Y. Meng, B.G. Thomas, Metall. Mater. Trans. B 34 (5) (2003) 685–705.
[19] K.C. Mills, A.B. Fox, ISIJ Int. 43 (10) (2003) 1479–1486.
[20] A.E. Huespe, A. Cardona, V. Fachinotti, Comput. Methods Appl. Mech. Eng. 182 (2000) 439–455.
[21] R.W. Soaresa, M.V.A. Fonsecaa, R. Neumann, V.J. Menezesa, A.O. Lavinasc, J. Dweckd, Thermochim. Acta 318 (1998) 131–136.
[22] A. Yamauchi, T. Emi, S. Seetharaman, ISIJ Int. 42 (10) (2002) 1084–1093.
[23] Y. Meng, B.G. Thomas, Metall. Materials Trans. B. 34 (5) (2003) 707–725.
[24] X.S. Zheng, M.H. Sha, J.Z. Jin, Acta Metall. Sin. (Engl. Lett.) 19 (3) (2006) 176–182.
[25] K. Schwerdtfeger, Heat withdrawal in continuous casting of steel, in: A.W. Cramb (Ed.), The Making Shaping and Treating of Steel-Casting Volume, 11th ed., AISE Steel Foundation, Pittsburgh, 2003, p. 11.
[26] O. Volcova, H.P. Heller, D. Janke, ISIJ Int. 43 (11) (2003) 1724–1732.
[27] C. Li, B.G. Thomas, in: 85th Steelmaking Conference Proceedings, ISS, Warrendale, PA, (held in Nashville, TN), 2002, pp. 109–130.
[28] U.S. Yoon, J.K. Park, B.G. Thomas, I. Samarasekera, in: 85th Steelmaking Conference Proceedings, ISS-AIME, Warrendale, PA, 2002, pp. 245–257.
[29] K. Schwerdtfeger, Heat withdrawal in continuous casting of steel, in: A.W. Cramb (Ed.), The Making Shaping and Treating of Steel-Casting Volume, 11th ed., AISE Steel Foundation, Pittsburgh, 2003, p. 12.
[30] K. Schwerdtfeger, Heat withdrawal in continuous casting of steel, in: A.W. Cramb (Ed.), The Making Shaping and Treating of Steel-Casting Volume, 11th ed., AISE Steel Foundation, Pittsburgh, 2003, p. 13.
[31] C. Li, B.G. Thomas, TMS (2003) 385–392.
[32] C. Li, B.G. Thomas, in: Brimacombe Memorial Symposium, Vancouver, Canada, Met Soc., CIM, 2000, pp. 595–611.
[33] S.K. Choudhardym, D. Mazumdar, A. Ghosh, ISIJ Int. 33 (7) (1993) 764–774.
[34] M. Janik, H. Dyja, S. Berski, G. Banaszek, J. Mater. Process. Technol. 153–154 (2004) 578–582.
[35] H. Wang, G. Li, Y. Lei, Y. Zhao, Q. Dai, J. Wang, ISIJ Int. 45 (9) (2005) 1291–1296.
[36] C.A. Santos, J.A. Spim, A. Garcia, Eng. Appl. Artif. Intell. 16 (2003) 511–527.